Available online at www.sciencedirect.com
SCIENCE DIRECT®
International Journal of Mass Spectrometry 226 (2003) 379–395
International Journal of Mass Spectrometry
www.elsevier.com/locate/ijms

Comparison of detection selectivity in ion mobility spectrometry: proton-attachment versus electron exchange ionization☆

Roderick R. Kunz[a,*], William F. Dinatale[a], Paul Becotte-Haigh[b]

[a] *Lincoln Laboratory, Massachusetts Institute of Technology, 244 Wood Street, Lexington, MA 02420, USA*
[b] *Ion Track Instruments, 205 Lowell Street, Wilmington, MA 01887, USA*

Received 10 April 2002; accepted 10 February 2003

Abstract

Two types of ionization have been compared for ion mobility spectrometry. The first uses a β-emitter to initiate proton exchange between an amine reactive gas and the analyte, whereas the second is based on electron exchange between photo-generated radical cations and the analyte. The latter method uses a 266-nm microchip laser in combination with naphthalene vapor to form naphthalene radical cations via two-photon ionization. Under ideal conditions, the laser-based method selectively ionizes analyte molecules on the basis of their ionization potential whereas the former does so on the basis of their proton affinity. Analysis of both pure and complex mixtures of compounds, including a variety of controlled substances such as cocaine, result in different response characteristics that are dependent on the given type of ionization employed. This gives rise to the possibility that a single instrument package can be equipped with two drift tubes to provide simultaneous analysis via the two types of ionization and thereby improve the overall detection selectivity.
Published by Elsevier Science B.V.

Keywords: Multiphoton ionization; Ion mobility spectrometry; Chemical detection; Naphthalene; 266 nm laser

1. Introduction

1.1. Background

Ion mobility spectrometry (IMS) is an atmospheric pressure means to detect trace levels of chemical vapors [1]. Although the recorded ion mobility spectra are generally of low resolution, the portable size and robust design of IMS instruments have nevertheless allowed for its widespread commercial application to detect narcotics [2–4], explosives [2–4], chemical warfare agents [5], and industrial process chemicals [6], often under harsh operating conditions. The primary drawback of IMS, other than the limited resolution, is chemical interference that can occur when used in richly contaminated settings [7]. Although highly selective forms of ionization such as resonant multiphoton ionization could in principle circumvent these limitations, previous studies have found that the selectivity afforded by these techniques cannot be realized when operating at higher pressures where gas-phase collisions provide ample opportunities for

☆ The Lincoln Laboratory Advanced Concepts Program is supported principally by the Department of the Air Force. Opinions, interpretations, conclusions, and recommendations are those of the authors, and are not necessarily endorsed by the United States Air Force.

* Corresponding author. Tel.: +1-781-981-7812; fax: +1-781-981-4983.
E-mail address: kunz@ll.mit.edu (R.R. Kunz).

1387-3806/03/$ – see front matter. Published by Elsevier Science B.V.
doi:10.1016/S1387-3806(03)00108-8

charge exchange [8]. However, the high collision rates ($>10^8\ s^{-1}$) at atmospheric pressure mean that, in most cases, thermodynamic equilibrium is obtained between the ions and the neutrals in a very short period of time. This has been used as an advantage in ion mobility spectroscopy to selectively ionize whole classes of compounds by virtue of their collectively unique thermodynamic properties (i.e., high proton affinity or high electron affinity, for example) [9] and provides the basis for the selective detection of chemical classes in IMS.

It was the purpose of the current research to investigate the possibility of creating a two-channel IMS equipped with separate drift tubes each using different gas-phase ion chemistries thereby increasing selectivity [10]. Although conceptually similar IMS approaches have used either simultaneous detection of both positive and negative ions or else multiple positive-ion IMS channels using dopants of varying proton affinity to act as a proton affinity filter [11], this study looks at the simultaneous use of two positive-ion channels using different ionization mechanisms. Through the use of appropriate data fusion algorithms, the channel outputs could then be used to increase the specificity of the instrument and thus provide an improved means to detect vapors, such as those produced from controlled substances, in contaminated field settings. The main challenge was the identification of ionization pathways that are sufficiently different, despite the myriad of ion–molecule reactions, to make this approach attractive. We chose the standard existing ionization method for one "channel" and focused most of our effort on developing a complementary ionization mechanism. For this feasibility study, the two "channels" were actually stand-alone instruments.

1.2. Ionization method one: amine mediated proton-attachment chemical ionization (Am-CI)

For the detection of illegal drugs, the principle form of ionization currently in use produces positive ions by proton exchange mediated by an organoamine dopant ion. The ionization cascade is often initiated by either the radioactive β-emitter ^{63}Ni, or by a corona discharge. The reaction sequence is described as [1]

$$[\text{Carrier}]\ (>99.99\%) + [\text{Dopant}] \xrightarrow{\beta^-} \text{H}[\text{Carrier}]_n{}^+ + [\text{Dopant}] \quad (1)$$

$$\text{H}[\text{Carrier}]_n{}^+ + [\text{Dopant}] \leftrightarrow n[\text{Carrier}] + \text{H}[\text{Dopant}]^+ \quad (2)$$

$$\text{H}[\text{Dopant}]^+ + [\text{Analyte}] \leftrightarrow [\text{Dopant}] + \text{H}[\text{Analyte}]^+ \quad (3)$$

where the functional component of the carrier gas is typically nitrogen, often in combination with residual water, and the dopant gas is ammonia, methyl amine, dimethyl amine, or a similar compound. Ionization selectivity is obtained for compounds whose proton affinities are greater than that of the dopant gas through an equilibrium shift of Eq. (3) to the right; i.e., the equilibrium position of Eq. (3) is determined by the relative proton affinities of the dopant and analyte, respectively. Fortuitously, most illegal drugs exhibit proton affinities greater than the common dopants and are hence readily ionized using this technique. Although the overwhelming majority of common organic compounds are not ionized by this method, there are certain classes of compounds commonly found in field settings, such as the organonitrogen compounds (e.g., acridine), found in some petroleum-based materials at 0.1–2%, that are ionized by this method and act as interfering compounds for instruments based on this detection principle. This has been a limitation in the successful use of IMS in all deployment settings (i.e., on ships where petroleum products are prevalent) [7].

1.3. Ionization method two: multiphoton ionization of a reactive ion followed by charge exchange (MPI-CE)

The nature of the second form of ionization used in this study is less well studied in the context of ion mobility spectrometry. Certainly, the use of direct photoionization, either by single-photon ionization using continuous wave sources [12,13] or by multiphoton ionization using pulsed lasers [8,14–16] has

been previously demonstrated. Less common are reports of the use of photogenerated radical cations as reactant ions for electron-exchange ionization. This mechanism was the focus of an earlier study [8] and was identified as the reason for minimal selectivity in direct photoionization IMS. Specifically, the reported selectivity loss in direct photo-ionization is from electron exchange of the photo-generated ion with other chemicals in the analyte mixture that possess a lower ionization potential. This process can be described as

$$[\text{Dopant}] \xrightarrow{h\nu} [\text{Dopant}]^{\bullet +} + e^- \quad (4)$$

$$[\text{Dopant}]^{\bullet +} + [\text{Analyte}] \leftrightarrow [\text{Dopant}] + [\text{Analyte}]^{\bullet +} \quad (5)$$

where the equilibrium in Eq. (5) is determined by the relative ionization potentials between the dopant and the analyte [17].

1.4. The two-channel concept

The benefits of using a two-channel IMS equipped with separate drift tubes based on both proton affinity-based equilibria and ionization potential-based equilibria can be realized only to the extent that these thermodynamic parameters are unrelated. Fortunately, most compounds' proton affinities and ionization potentials are not related, or only loosely related at best. Both proton affinity [18] and ionization potential [19] data for a wide variety of organic chemicals have been tabulated. Plotting one value vs. the other (some of these values are shown later in Fig. 4) for a representative subset of common compounds selected from those tables gives very poor correlation ($R^2 = 0.15$), hence our assertion that ionization dominated by one mechanism or the other should provide complementary detector responses. The challenge in the current study is to identify the extent to which competing ionization pathways take part in dictating the overall ionization selectivity of a given channel, as this would be the primary limitation to realizing the proposed benefits of this approach.

2. Experimental

2.1. IMS detector based on ^{63}Ni ionization—"Am-CI"

The IMS channel using ^{63}Ni ionization and amine-based reactive gas chemistry was an Itemizer® Ion Trap IMS provided by Ion Track Instruments and it was used as received. It was configured for narcotics mode (positive ion detection) and used ammonia as the reactive gas. The reactive gas concentration, sample flow rate, drift tube counterflow, and operating temperatures were ∼3 ppm, ∼100 sccm, ∼150 sccm, and 200 °C, respectively and were preset at the factory and not varied as part of this study.

2.2. IMS detector based on multiphoton ionization–chemical ionization at 266 nm—"MPI-CE": hardware

The IMS channel using photoionization was a custom modified Mark II® instrument provided by Ion Track Instruments. The modifications involved removal of the ^{63}Ni ionization chamber and replacing it with a resonant optical cavity consisting of two parallel dielectric mirrors, coated for normal-incidence 266-nm reflection and spaced approximately 1-cm apart. An ion reflector plate was inserted orthogonal to and between the mirrors, parallel to and about 0.5 cm away from the entrance grid to the drift tube. This plate was wired to the Mark II's power supply such that is was at the same potential as the entrance grid between pulses (creating a field free "ion trap") and was positive relative to the grid for initiating the ion drift spectrum [2]. A 1/8 in. o.d. sample line was inserted through an end plate into the space between the reflector plate and the entrance grid such that the ionization chamber was a volume approximately 1 cm wide × 0.3 cm high × 1 cm long. The only place that gas could exit was through the drift tube and through a small opening for the laser beam. Other than the ionization chamber, the drift tube geometry and electric fields were approximately the same for all experiments in both devices unless

otherwise noted. The drift tube electric field for both instruments was ∼220 V/cm but slight differences in drift time were observed between the two stemming from difference in temperature and ionization region geometry.

The carrier gas was nitrogen at a flow rate of 105 sccm. The counter flow was also nitrogen and its flow rate was 240 sccm. The nitrogen was obtained by liquid nitrogen boil off and delivered to the instrument using electropolished stainless steel tubing. The oxygen level was <10 ppb and the water level was 35 ± 5 ppb, but the levels measured near the drift tube were as high as ∼200 ppb at times due to adsorption of moisture on the inside of the delivery lines following system maintenance. The moisture levels were determined by both an Edgetech Dewtrace Model 1-C Trace Moisture Analyzer and by a Meeco Aquavolt + sensor. Experiments were also tried using dry air (water < 50 ppb) as both the carrier and counter flow gases and no differences in the response sensitivities were observed. As a result, for simplicity, nitrogen was used unless specified otherwise. The drift tube operating temperature was 220 °C.

The laser used was a custom manufactured microchip ultraviolet laser [20]. The laser head consisted of a Nd:YAG solid state laser operating at 1064 nm along with the necessary crystals to produce the second harmonic at 532 nm and the fourth harmonic at 266 nm. The output energy per pulse at 266 nm was 8–12 μJ and the repetition rate was varied from between 0.5 and 3 kHz. With a beam diameter of only 0.02 cm and a pulse duration of ∼200 ps, the peak power density at the output of the laser head was in excess of 10^8 W/cm^2. This is high enough to provide near unit quantum efficiency for multiphoton ionization of many strongly absorbing aromatic compounds [21]. Physically, the laser head was only 3 in. long × 1 in. in diameter and was connected via a fiber optic link to an infrared diode laser, which acted as the optical pump. The optical pump was an 808-nm diode laser manufactured by Limo Laser. These microchip lasers can be quite robust and have been deployed in a variety of field applications [22].

2.3. IMS channel based on multiphoton ionization–charge exchange ionization at 266 nm—"MPI-CE": reactive gases

Several reactive gases were initially tried, including aniline, xylene, azulene, and naphthalene. The most critical desired property was a low enough ionization potential to enable facile multiphoton ionization. The two-photon energy at 266 nm is 9.2 eV. The ionization potentials for the listed dopant gases [19] were azulene (7.4 eV), aniline (8.05 eV), naphthalene (8.15 eV), and xylene (8.57 eV), which are all below 9.2 eV. Another desirable property is to have a low proton affinity to avoid activation of parallel ionization pathways dominated by proton attachment. In this regard, the desirability order in ascending values of proton affinity [16] was xylene (8.4 eV), naphthalene (8.47 eV), aniline (9.1 eV), and azulene (9.56 eV). Another consideration is the absorption coefficient and excited-state lifetimes of each of these compounds at 266 nm, as it has been reported that these factors figure prominently in two-photon ionization probabilities [23]. In this regard, the polycyclic compounds naphthalene and azulene appear most desirable as they both have very strong one-photon absorption coefficients at 266 nm. When considering all these factors, we chose naphthalene as our dopant gas and all data presented was obtained using this gas. Naphthalene efficiently undergoes multiphoton ionization under our conditions. Given the relatively long lifetime of the intermediate excited state [24] (∼200 ns) and based on previous reports of naphthalene multiphoton ionization [21,25], we expect the overall photoionization efficiency to be between 1 and 10%.

2.4. Test reagents

All regular test chemicals were purchased from Aldrich Chemical and used as received. The controlled substances were obtained from Cerilliant as solutions in methanol and/or acetonitrile and were either used as received or diluted in the appropriate research grade solvents mentioned above. The naphthalene reactive gas used for initiating electron-transfer ionization

was received enclosed in a calibrated permeation tube from VICI Metronix and the tube was heated to between 100 and 130 °C. It was calibrated at the factory for a permeation rate of 2377 ng/min at 100 °C. Using our carrier flow of 105 sccm, this corresponded to 4 ppm of naphthalene. At temperatures between 110 and 130 °C, the permeation rate was not calibrated but we expect the naphthalene concentration increased to between 6 and 10 ppm. For most of the presented data, a temperature of 130 °C was used, corresponding to a naphthalene concentration of ∼10 ppm.

2.5. Sample introduction and measurement

Each detector was equipped with the standard Ion Track Instruments thermal desorber designed for use with 3 in.-round cloth wipes. Rather than use cloth wipes that may irreversibly adsorb some of the test chemicals, we used thin aluminum (∼100 μm thick) disks of the same diameter. Solid samples were prepared by placing microliter quantities of solutions of various dilution onto the aluminum disk followed by evaporation of the solvent on a hotplate. After evaporation, the disk was introduced into the instrument for thermal desorption of the analyte. This procedure was used for the 22 solid samples of the 27 total samples tested. The five liquid samples were introduced into the instruments by direct injection of small (∼microliter) neat quantities (benzene and toluene) or liquid–liquid solutions (pyridine, pyrazine, and 1,4-diaminobutane). Typical solvents were acetonitrile, diethyl ether, and methanol, with acetonitrile being the preferred solvent. The use of solvents raised potential concerns regarding their participation in charge-exchange reactions, but we first tested the solvents neat to determine their propensity to charge exchange with the dopant. At the injection sizes we used, we typically observed very weak (less than typical analytes) signal. This is because nearly all the compounds tested had higher proton affinity than the solvents. Finally, the measurement of mixtures of cocaine and several petroleum-based products were all done neat (from the aluminum disks) and hence solvent contributions were non-existent for those experiments.

Upon placement of the aluminum disk in the desorber, the resultant temperature ramp caused the sample to heat, desorb, and be drawn into the inlet by an air diaphragm pump. After being drawn into the air inlet, some fraction of the sample struck and diffused through the heated inlet membrane and entered the nitrogen carrier gas stream. This is the standard inlet design for Ion Track Instruments commercially available units and has been described elsewhere [2]. For analysis of mixtures, we used the process just described but now employed a two-step sample application to the aluminum disk. For example, in order to examine the impact of a 1000-fold higher level of contaminant we would first apply 10 ng of cocaine followed by 10 μg of the contaminant. In this way we could examine the degree to which chemical interference occurs for the two ionization types.

2.6. Data acquisition and derivation of sensitivity factors

For each sample introduced into either instrument, the total signal generated as a function of the injection mass was recorded. The total signal detected (in C) for a given injection is given by

$$\text{Total signal (C)} = \frac{ARt_{\text{res}}}{G}$$

where A is the integrated peak area (in V-s) in a single given ion mobility spectrum, R is the rate at which these scans are obtained (in s^{-1}), t_{res} is the sample residence time in the instrument and is determined by the desorption profile of the compound (in s) (usually between 2 and 30 s and limited by adsorption on tubing walls), and G is the preamplifier gain in V/A ($G = 10^8$ V/A for these measurements). The sensitivity factor is then obtained from

$$\text{Sensitivity (C/mol)} = \frac{\text{Total signal}}{\text{Number of moles injected}}$$

For more accurate determination of the sensitivity factors, multiple injections were performed over a range of injection sizes and the total signal (in mC) was plotted vs. the injection size (in mol). The slope of the graph yielded the sensitivity.

3. Results

3.1. Dopant ions produced by multiphoton ionization: naphthalene

The commercial maturity of the instrument used for Am-CI allowed for a straightforward evaluation, but the experimental nature of MPI-CE led us to investigate in greater detail its ionization processes.

Naphthalene has a very high one-photon absorption cross-section at 266 nm of $\sim 2 \times 10^{-17}$ cm^2 (ref. [26]) likewise, it is possible that the excited-state and/or radical cationic form of naphthalene may absorb the 532 nm light as well. Although it has been reported that visible radiation (~560 nm) can influence photo-ion fragmentation during the UV-induced multiphoton ionization of substituted aromatics [27], we made no attempt to either limit the amount of 532 nm light in the ionization chamber or study the impact it had on our mobility spectra. Nevertheless, the illumination intensity of 266-nm radiation alone allowed for high ionization efficiency and would result in severe peak broadening if the naphthalene concentration was not limited to less than a few parts per million. This behavior is consistent with that described in previous, similar experiments [16]. Although molecular fragmentation is not expected from two-photon ionization at 266 nm, we observed two peaks in the MPI mobility spectrum of naphthalene at reduced mobilities of roughly 1.8 and 2.2 cm^2/V-s, respectively (Fig. 1). We were able to determine that the lifetime of the ion at a mobility of 1.8 cm^2/V-s was considerable shorter than that for the ion at 2.2 cm^2/V-s; we estimate the latter was on the order of the ion extraction pulse (0.2 ms).[1] The value of 1.8 cm^2/V-s agrees well with the published values for naphthalene of 1.85 cm^2/V-s [28]. Based on the slightly higher mobility of the second peak, we expect it to be a C_7 or C_8 compound, possibly the radical cation of bicyclo[4.2.0]octa-1,3,5,7-tetraene formed by the electrocyclic reaction of the intermediate product formed from acetylene elimination. Although fragmentation such as this is not expected from straightforward two-photon ionization, excited state absorption or 2 + 1 ionization processes involving the 10-fold more intense 532-nm radiation may contribute to these more energetic processes. Further, when a compound was introduced that had a lower ionization potential than naphthalene, it was the ion at 2.2 cm^2/V-s whose signal decreased first due to charge exchange neutralization, indicating either that that compound had a lower ionization potential than naphthalene or that the relative lifetimes play an important role in the ion-exchange kinetics. We cannot speculate further on the reason for this, but we can note that bicyclo[4.2.0]octa-1,3,5,7-tetraene has an ionization potential well below that of naphthalene (7.87 eV vs. 8.15 eV for naphthalene) [19].

3.2. Sensitivity factors of pure compounds

The simplest way to compare the two detectors relative characteristics was to measure a number of pure compounds whose ionization potentials and proton affinities were known, along with additional compounds of more practical interest such as selected narcotics, whose proton affinities and ionization potentials have not yet been reported. This was done for nearly 30 chemicals of which several sample spectra are shown in Fig. 2, and of which several sample calibration curves used to derive the detection responses appear in Fig. 3. Table 1 and Fig. 4 summarize these experiments, where Table 1 lists the resulting sensitivity factors for all the compounds, Fig. 4(a) plots the compound's responses to Am-CI as a function of that compound's ionization potential and proton affinity

[1] We determined that the two observed naphthalene peaks had different lifetimes by varying the phase difference between the laser pulse (200 ps pulse duration, 2 ms between pulses at 500 Hz) and the ion extraction pulse (0.2 ms duration, 25 ms between pulses) and by watching the ratio of the two peaks. When the laser pulse was immediately prior to or during the ion extraction pulse, the peak at 1.8 cm^2/V-s was at a maximum. When the laser pulse preceded the ion extraction pulse by a maximum amount, nearly the full laser pulse period of 2 ms, the peak at 1.8 cm^2/V-s was at a minimum—less than half its maximum value. During these observations, the peak at 2.2 cm^2/V-s did not change. From these observations, we estimate that the 1.8 cm^2/V-s peak had a lifetime of a few ms whereas the 2.2 cm^2/V-s peak was at least many ms.

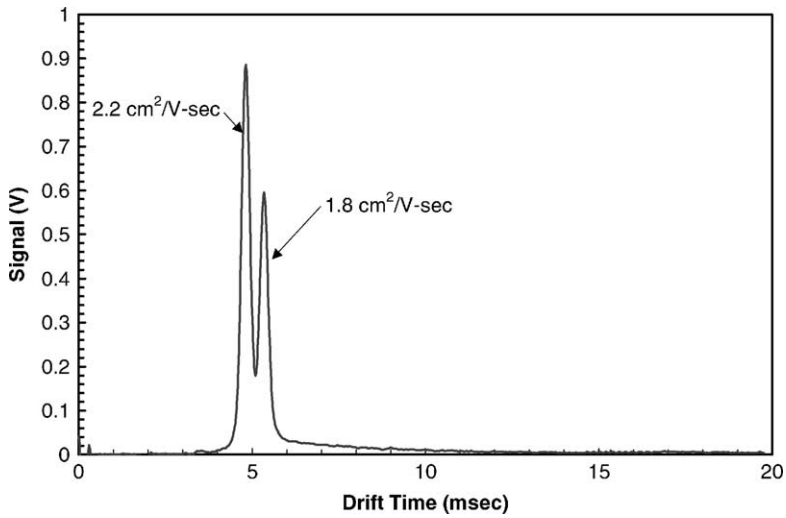

Fig. 1. Spectra of the laser-ionized naphthalene reactive gas used to induce chemical ionization of analyte compounds. The two peaks are thought to be naphthalene (5.4 ms) and a possibly a C7 or C8 fragment of naphthalene (see text).

(in the cases where these values were available), and Fig. 4(b) plots the compound's responses to MPI-CE, also as a function of each compound's ionization potential and proton affinity. Finally, Fig. 4(c) summarizes the work by looking at the ratio of responses of one ionization method to the other. Of these results, Fig. 4(a) and (b) most clearly indicate the "purity" of the ionization process and are two-dimensional analogs of plots previously made of ion yield vs. ionization potential made for benzene-mediated charge-exchange ionization of other substituted aromatics [30]. For example, in Fig. 4(a), where ionization is via proton exchange, the detector response should only depend on the analyte's proton affinity and be independent of its ionization potential. From Fig. 4(a), this is apparent, with all the response contours running parallel to the *x*-axis and hence indicating little dependence on the analyte's ionization potential. Likewise, the sensitivity of Am-CI to these compounds varies by roughly five orders of magnitude over the range of proton affinities available to test. In contrast, Fig. 4(b) shows the results for MPI-CE, where the response contours are no longer horizontal, indicating a detector response that is dependent on the analyte's ionization potential. Interesting to note from Fig. 4(b), however, is the absence of a detector response that is completely independent of proton affinity (i.e., the response contours do not run strictly parallel to the *y*-axis). This can only mean that ionization pathways other than electron exchange remain active, and this appears to be most marked for those compounds whose ionization potentials are much greater than naphthalene's. Nevertheless, Fig. 4(b) does show that MPI-CE is different from Am-CI and this is further illustrated in Fig. 4(c), where the ratio of the responses from the two channels are plotted for the same set of chemicals. From this, we now see that the proton-affinity-based ionization (Am-CI) is >1000 times more sensitive to small cyclic amines such as pyridine and pyrazine, to 15 times more sensitive to polyethers, whereas the laser-induced chemical ionization (MPI-CE) is >5 times more sensitive to polycyclic aromatics such as pyrene and dibenz(*a*,*h*)anthracene.

3.3. Semi-empirical model for detector responses to pure compounds

The data in Table 1 summarizes the IMS detector responses for all the chemicals tested. Of these chemicals, roughly half of them have both their ionization

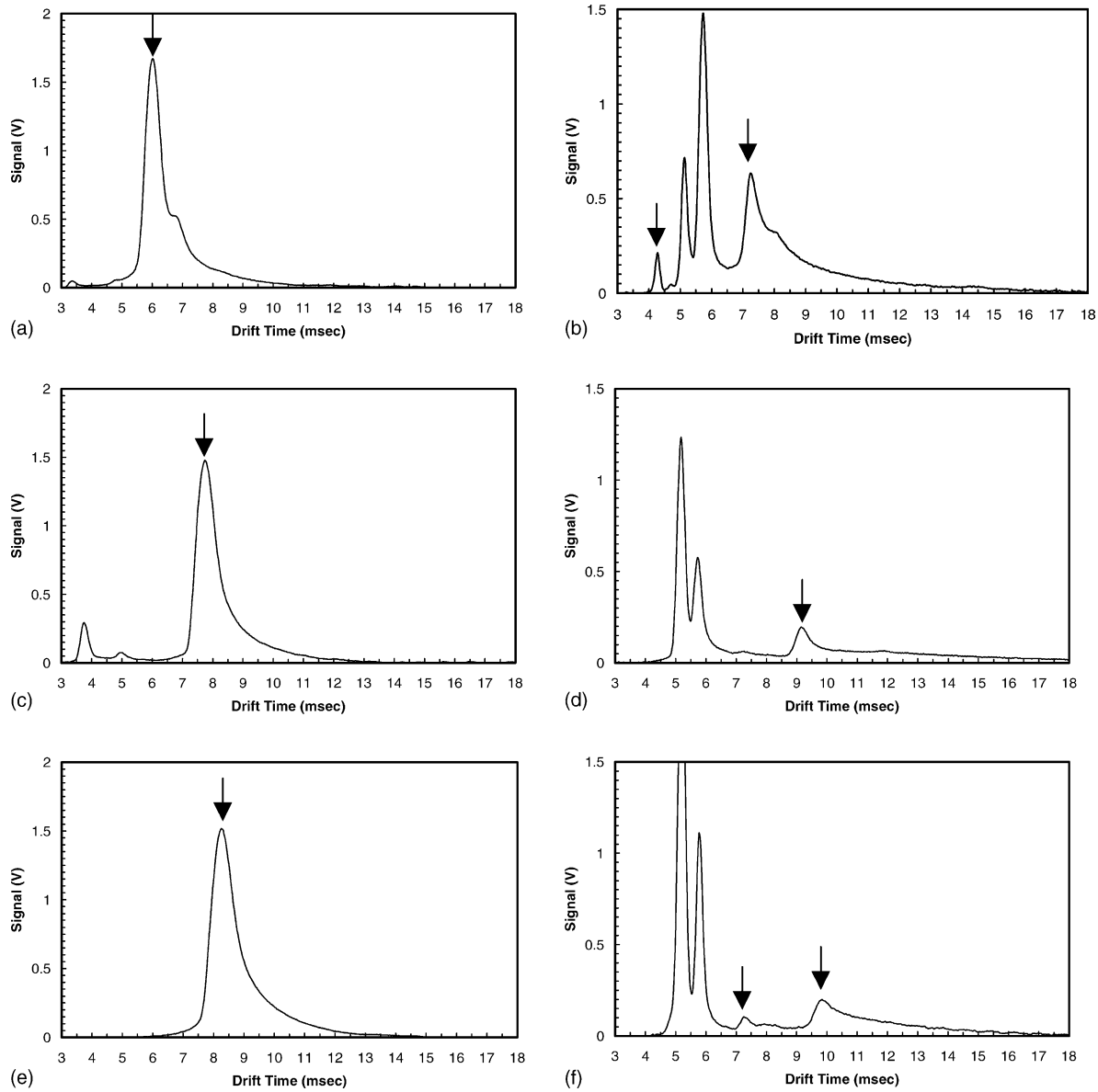

Fig. 2. Representative ion mobility spectra of pure compounds: (a) methylenedioxy-methamphetamine detected using $^{63}Ni/NH_3$ proton exchange ionization (Am-CI); (b) methylenedioxy-methamphetamine detected using laser/naphthalene MPI electron exchange ionization (MPI-CE); (c) cocaine detected using Am-CI; (d) cocaine detected using MPI-CE; (e) lysergic acid diethylamide detected using Am-CI; (f) lysergic acid diethylamide detected using MPI-CE. In each of these spectra, the analyte peak(s) is indicated by the arrow. These are representative spectra, no particular care was taken to ensure the injection sizes were the same for all cases, as a result the size of the analyte peaks and the reactive ion peaks (unmarked) vary from spectra to spectra.

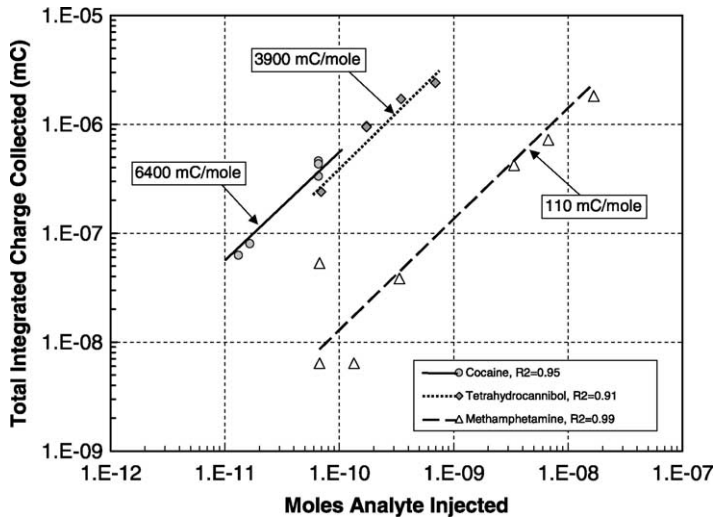

Fig. 3. Examples of the calibration curves used to derive the response sensitivities as a function of ionization method. The *y*-axis values are the total integrated charge collected, integrated over both drift time and the total time each chemical took to pass through the instrument.

potentials and proton affinities reported in the literature. Using this subset of materials, it is possible to relate each chemical's normalized detector response to the difference in ionization potential between the naphthalene and the analyte for the MPI-CE or, for Am-CI, between the difference in proton affinity of the ammonia and the analyte. Fig. 5 shows the results of this relationship for 12 of the 27 chemicals tested. Since the detected signal is proportional to the equilibrium of the generic reaction

$$A + D^+ \rightarrow A^+ + D \tag{6}$$

where A is the analyte and D is the dopant, we can say that, in the most generic sense

$$\text{Analyte A signal} \propto K_{eq} = \frac{[A^+][D]}{[A][D^+]} \tag{7}$$

where the equation

$$\frac{[A^+][D]}{[A][D^+]} = \exp\left(\frac{-\Delta G}{kT}\right) \tag{8}$$

describes the relationship between the reaction's free energy change and its equilibrium constant, and was used previously to actually determine values for proton affinity [18]. Since our reported sensitivities are in terms of the analyte ion concentration $[A^+]$ per unit of analyte A introduced into the instrument (results in Table 1), we can say that

$$\text{Measured analyte A signal} \propto \frac{[A^+]}{[A]+[A^+]} \sim \frac{[A^+]}{[A]}, \quad \text{for } [A^+] \ll [A] \tag{9}$$

and Eq. (8) can be rearranged to more accurately reflect our reported values

$$\text{Reported analyte signals from Table 1} \propto \frac{[A^+]}{[A]} = \frac{[D^+]}{[D]} \exp\left(\frac{-\Delta G}{kT}\right) \tag{10}$$

Unfortunately, the quantitative application of Eq. (10) is limited for these experiments due to factors that control the exact reagent concentrations (differences in inlet membrane diffusion, wall equilibration, etc.). However, we might still expect the measured signal to have the basic form of a simplified version of this expression

$$\text{Reported analyte signals from Table 1} = \exp(a\,\Delta G^* + b) \tag{11}$$

where ΔG^* is proportional to the reaction free energy and is given by the difference in either the analyte and

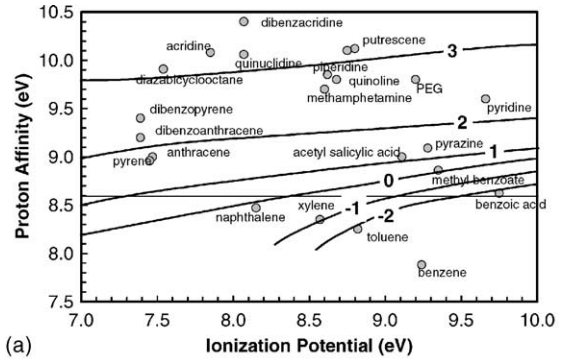

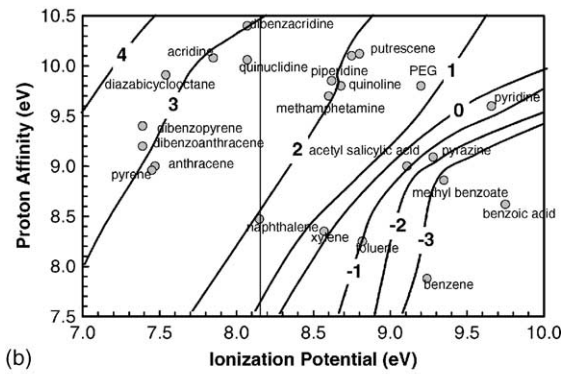

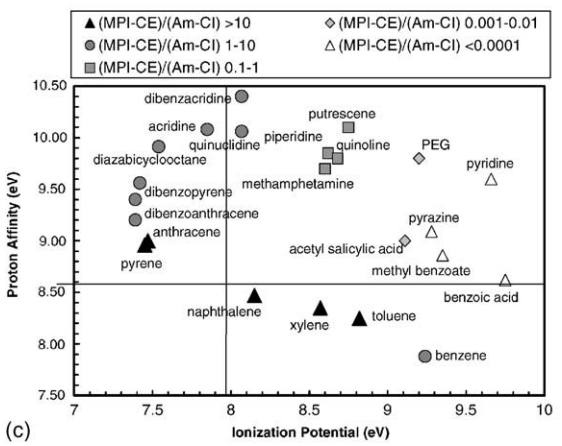

Fig. 4. (a) Response contours for $^{63}Ni/NH_3$ proton exchange ionization (Am-CI). All interpolated contour lines are in units of log(response) (mC/mol). If the signal depended only on analyte proton affinity, all contour lines would run horizontally and the detector response would be near zero at proton affinities less than 8.6 eV (the value for NH_3, the thin horizontal line). (b) Response contours for laser/naphthalene MPI electron exchange ionization (MPI-CE). If the signal depended only on the analyte ionization potential, all contour lines would run vertically and the detector response would be near zero at ionization potentials greater than 8.2 eV (thin vertical line). The more horizontal contour lines at ionization potentials >9.5 eV indicate that proton exchange is beginning to dominate in this region, even though absolute sensitivities are low. The contours in (a) and (b) are derived from the values in Table 1. (c) Data points showing the ratio in detector responses for two methods.

naphthalene ionization potentials (for MPI-CE) or the difference in the ammonia and analyte proton affinity (for Am-CI), and a and b are fitting parameters dependent on the concentration of dopant (or interfering chemicals). Note that the use of this expression is limited to pure compounds measured over relatively narrow ranges in concentration. However, using this expression, the curve fits in Fig. 5 yield $a = -5.50$, $b = -5.66$ for MPI-CE and $a = -4.86$, $b = -2.29$ for Am-CI. The response selectivity, defined as the signal ratio between the two ionization methods is now simply

$$\text{Response selectivity} = \frac{\exp(a_{\text{MPI-CE}}\,\Delta G^*_{\text{MPI-CE}} + b_{\text{MPI-CE}})}{\exp(a_{\text{Am-CI}}\,\Delta G^*_{\text{Am-CI}} + b_{\text{Am-CI}})} \quad (12)$$

which simplifies to

$$\text{Response selectivity} = \exp[-\alpha(\Delta G^*_{\text{MPI-CE}} - \beta\,\Delta G^*_{\text{Am-CI}}) + k] \quad (13)$$

where $\alpha = 5.5$, $\beta = 0.88$, and $k = -3.37$. The experimentally measured selectivity values are plotted in Fig. 6 vs. the semi-empirically derived selectivity (Eq. (13)) with a residual R^2 value of 0.68. The scatter in the data is fairly large and is likely due to factors such as competing ionization pathways or due to factors unrelated to ionization thermodynamics, such as differences in diffusion rates through the inlet membrane or variations in analyte concentration. Nevertheless, it is apparent that by comparison of the ΔG^* values for any given analyte for each ionization method, a qualitative sense of the expected selectivity can be obtained. This might allow for design of multichannel IMS instruments that target specific analytes.

Table 1
A summary of instrument responses for each of the two ionization types investigated

Compound	Am-CI			MPI-CE		
	Mass range (ng)	Response (mC/mol)	R^2	Mass range (ng)	Response (mC/mol)	R^2
Benzene	10^7	0.0	N/A	10^6–10^7	0.005 ± 0.003	0.24
Pyridine	50–2000	590 ± 46	0.89	10^4–10^5	0.190 ± 0.03	0.36
Pyrazine	2000	1.8	N/A	1000–25000	0.005 ± 0.0004	0.35
1,4-Diaminobutane	44–2200	3100 ± 720	0.29	1000–3000	37 ± 3	0.89
Toluene	10^6	0.002	N/A	1000	0.097	N/A
Naphthalene	1000	0.8	N/A	N/A	N/A	N/A
Quinoline	20–1000	340 ± 310	0.08	50–1000	37 ± 1	0.98
Methamphetamine	20–200	180 ± 14	0.96	5–20000	110 ± 2	0.99
(*S*)-Nicotine	200–1000	210 ± 80	0.81	20–1000	430 ± 36	0.93
Anthracene	20–5000	36 ± 30	0.20	2–5000	430 ± 6	0.99
Acridine	200–1000	960 ± 110	0.96	2.5–50	890 ± 200	0.26
Acetyl salicylic acid	750–2000	35 ± 21	0.17	25000	<0.001	
Phenylpropanolamine	20–2000	170 ± 70	0.69	100–2000	270 ± 29	0.82
Methylenedioxy-methamphetamine	50–500	2000 ± 180	0.94	20–5000	120 ± 4	0.99
Ecgonine methyl ester	200–500	660 ± 230	0.89	5–500	650 ± 29	0.86
Poly(ethylene glycol)	1000	660	N/A	104–106	48 ± 25	0.28
Pyrene	500–1000	29 ± 20	0.28	10–15000	220 ± 5	0.99
Phencyclidine	100–1000	460 ± 150	0.80	5–200	1800 ± 48	0.97
Dibenz(*a*,*h*)anthracene	10–1000	670 ± 10	0.99	5–200	3200 ± 580	0.33
Dibenz(*a*,*h*)acridine	1000	4300	N/A	0.4–100	6900 ± 780	0.99
Morphine	20–2000	1400 ± 600	0.30	3–40	5400 ± 290	0.87
Benzoyl ecgonine	200–500	1100 ± 900	0.37	5–500	4600 ± 59	0.99
Tetrahydrocannibol	200–500	5400 ± 500	0.99	20–2000	3900 ± 190	0.91
Cocaine	20–200	16000 ± 4000	0.94	4–1000	6400 ± 290	0.95
Lysergic acid diethylamide	200–500	910 ± 750	0.14	20–1000	9200 ± 390	0.92
6-Acetyl morphine	50–200	2400 ± 160	0.93	2–40	1200 ± 480	0.06
Heroin	200–500	3400 ± 300	0.99	5–100	3100 ± 380	0.29

The first column lists the chemicals tested. Under each type of ionization, the left-most column indicates the range of sample sizes used, the center column is the response derived from calibration curves where the error is the residual error in the slope for the curve fit, and the right-most column is the residual R^2 value for the curve fits. In instances where the R^2 value is less than 0.80, the sensitivity is computed from the mean value and the error limits represent the standard deviation. An R^2 value of N/A indicates only a single sample was used in the test.

3.4. Analysis of mixtures: simulated target/interference combinations

To further compare the different types of ionization, a test was performed where measurements were made in the presence of large amounts of potential interfering compounds. For this study, three interfering substances were examined, standard-grade diesel engine fuel, ATF3 transmission fluid, and diesel-engine motor oil. These are designated contaminants A, B, and C, respectively; and have been identified as having a small fraction of high-proton-affinity organonitrogen compounds [7] and thus have historically been known to act as interferants. Because the exact fraction of these mixtures comprised of heterocyclic organonitrogen compounds was not known, no quantitative model of interference could be derived. Nevertheless, these experiments were of practical interest and allowed for some qualitative conclusions.

Our experiments involved introducing 10 ng of cocaine free base along with increasing amounts of the interfering substance and comparing the results for the two detectors. Fig. 7 shows the results for each device for each of the three interfering substances. In each case the cocaine signal (7.8 ms in Fig. 7(a), (c), and (e) and 8.7 ms in Fig. 7(b), (d), and (f)) becomes

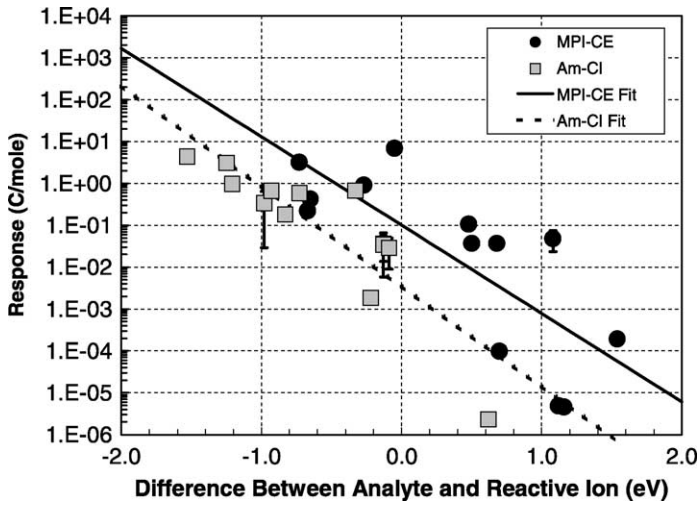

Fig. 5. Plots of detector response as a function, for MPI-CE, of the difference in ionization potential between the analyte and dopant, and, for Am-CI, the difference in proton affinity between the dopant and the analyte. The data points represent response values derived from linear fits of signal vs. concentration (at concentrations where they are linearly related). The solid curves are fits to the data and are discussed in the text.

obscured by the increasing levels of charge exchange as the interfering substances' concentrations increase. Fig. 8 summarizes the results from Fig. 7, where the cocaine signals as a function of interfering compound over-concentration are plotted. From Figs. 7 and 8, it is clear that although both ionization schemes are affected by the presence of overwhelming amounts of interfering chemicals, the two ionization methods manifest this contamination in different ways. Different components within these mixtures are ionized using each method, and the rate at which charge exchange between the cocaine and these ionized contam-

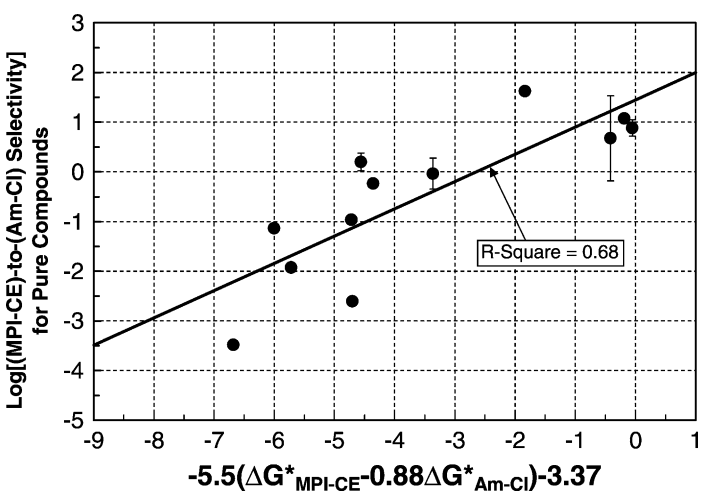

Fig. 6. A plot of the measured selectivity between MPI-CE ionization and Am-CI ionization for a selected subset of the pure chemicals vs. the derived expression for selectivity (see text for discussion).

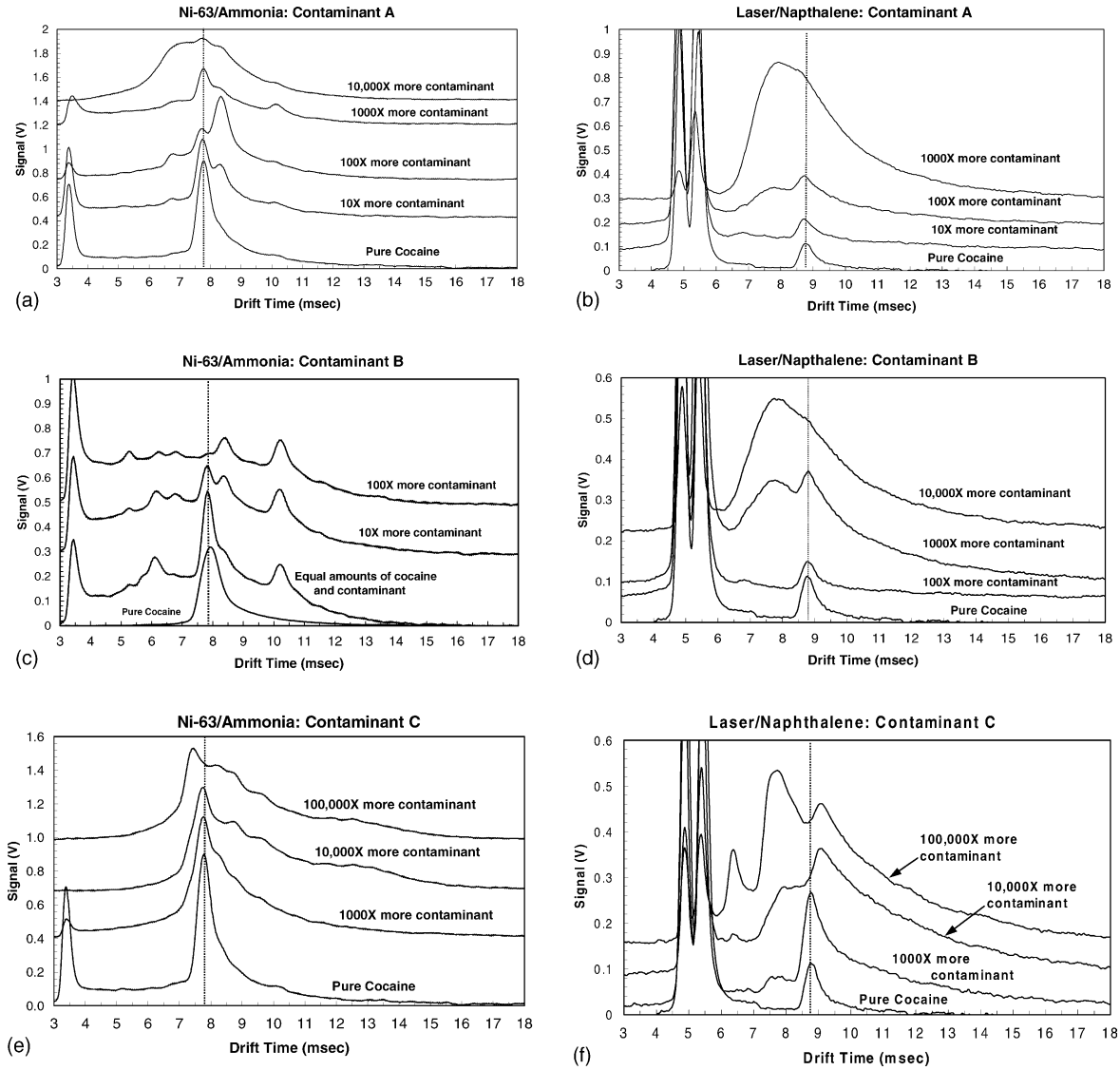

Fig. 7. (a, b) Comparison of the two ionization methods' responses when challenged with large amounts of contaminant A (diesel fuel) in the presence of 10 ng of cocaine. The very broad peak in the laser/naphthalene channel is due to coulombic repulsion of ions directly ionized by the laser. (c, d) Comparison of the two ionization methods' challenged with large amounts of contaminant B (ATF3 fluid) in the presence of 10 ng of cocaine. (e, f) Comparison of the two ionization methods' challenged with large amounts of contaminant C (diesel oil) in the presence of 10 ng of cocaine. The slight differences in drift times between the two methods are discussed in the text.

inants is different as well. Note the very broad peaks in Fig. 7(b) and (d), indicating charge broadening of the peaks due to the large amount of direct photoionization of the interfering compound. In fact, this direct photoionization of the interfering compound actually *increased* MPI-CE's sensitivity at intermediate levels of interfering substance as a result of charge exchange between the contaminant and the analyte (Fig. 8(c)).

Fig. 8 shows several qualitative trends. First, for Am-CI, the impact of increased interferant concentra-

tion has a monotonic effect on analyte signal reduction, whose slope presumably depends on the ΔG^* for the analyte–interferant pair. Quantitative evaluation of this behavior using known interferences would have allowed prediction of analyte-signal loss as a function of interferant concentration and proton affinity, but unfortunately was beyond the scope of this current study. For the interferant mixtures used here, one can see the difficulties associated with operating a conventional IMS around these petroleum-based vapors, except perhaps for interferant C (diesel fuel) which is presumably the most refined of the three petroleum products tested and hence least likely to be contaminated with organonitrogen compounds. However, the behavior of

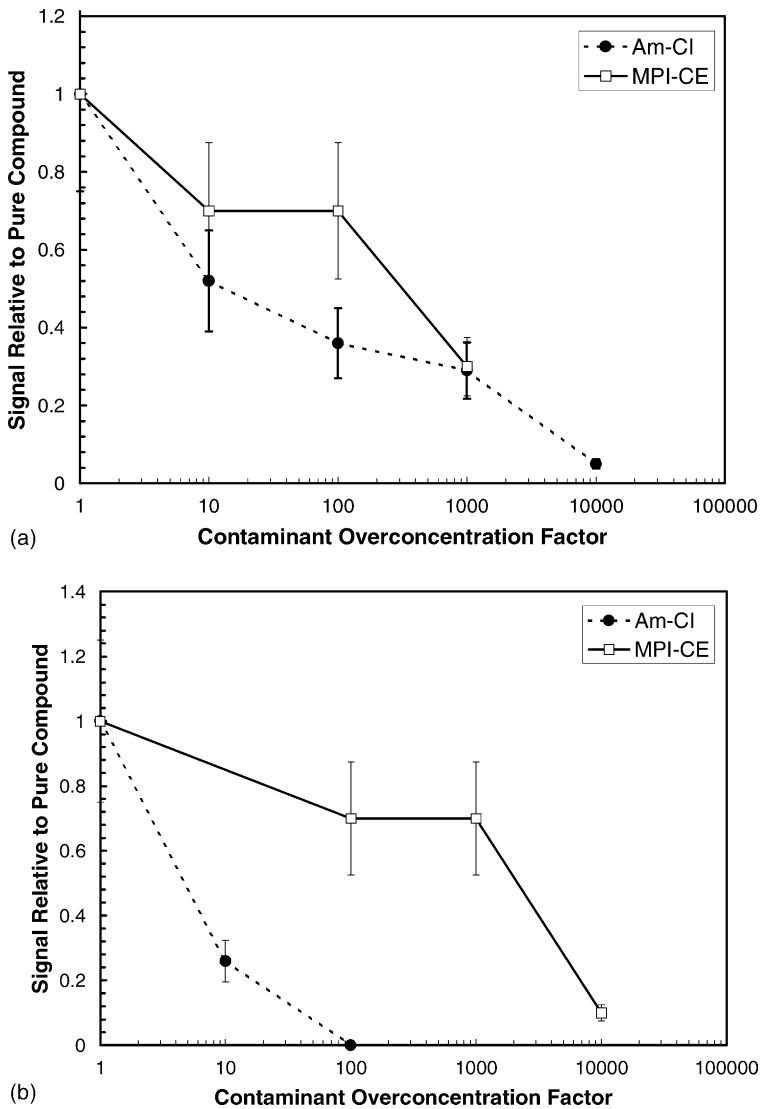

Fig. 8. A summary of: (a) Fig. 7(a) and (b) showing the reduction in cocaine signal as a function of contaminant A (diesel fuel); (b) Fig. 7(c) and (d) showing the reduction in cocaine signal as a function of contaminant B (ATF3 fluid); and (c) Fig. 7(e) and (f) showing the reduction in cocaine signal as a function of contaminant C (diesel oil). The lines are drawn simply to guide the eye.

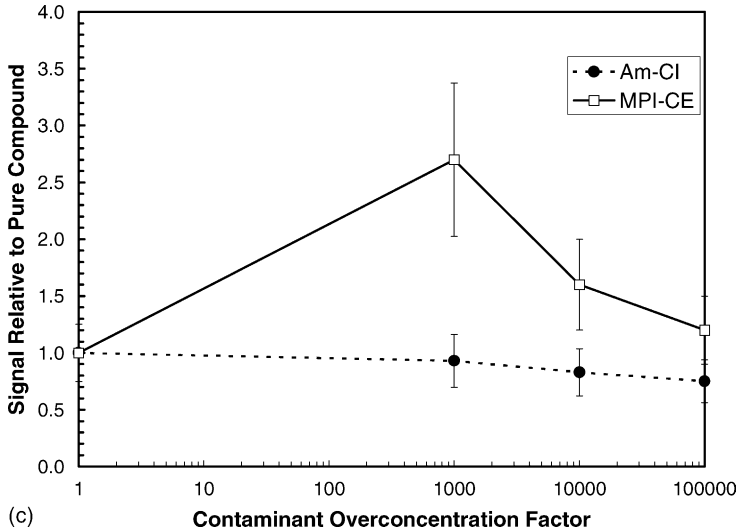

Fig. 8. (*Continued*).

the MPI-CE is made more complex by the direct photoionization of the interferant (mixture C, diesel fuel) which had the effect of increasing both the analyte and the naphthalene signals through charge exchange. Introducing diesel fuel vapors to the MPI-CE IMS was the effective equivalent of increasing the dopant concentration and actually had a beneficial effect. For mixtures A and B, the presence of nitrogen-containing compounds (confirmed by Am-CI) acted to neutralize the analyte ions as these compounds exhibit low ionization potentials in addition to their high proton affinities.

4. Discussion

The idea behind expanding an instrument from one to two or more channels is to improve detection selectivity, increase noise rejection, and ultimately to increase the operator's confidence in a reported alarm. As the number of detector channels increase, the absolute detection selectivity needed in each channel decreases. An extreme example of this are the artificial noses comprised of arrays of relatively non-selective sensing elements [29]. Straightforward implementation of multi-channel sensors requires that each channel's response is simply the linear addition of the individual analytes' responses. In IMS, this is rarely the case due to signal reduction stemming from charge neutralization and other artifacts associated with charge exchange (peak broadening, cluster formation, etc.). Given this, implementation of a multi-channel IMS may likely require more complex forms of signal processing than other forms of multi-channel analysis. For this reason it is worthwhile to take a closer look at the characteristics governing both the similarities and differences between the two ionization methods tested in this study.

From Fig. 4(b), it is apparent that, for the MPI-CE, the ionization is not strictly determined by the ionization potential of the analyte molecule. This is clearly a result of the presence of parallel ionization pathways. What is less clear, however, is whether these competing reactions in the laser-based channel represent proton-exchange chemistry activated by the presence of trace levels of water or whether these competing reactions are inherent to the reactive gas chemistry and are thus more fundamental in nature. Our current feeling is that trace water may play an important role in initiating proton-exchange reactions in the MPI-CE, despite our best efforts to minimize its concentration. Certainly, it is not practical to imagine operating in

the complete absence of any residual water vapor and therefore, it is expected that some degree of proton exchange ionization will always occur, regardless of the desired or intended primary ionization mechanism. Nevertheless, even marginally different response characteristics between different detector channels may be useful as has already been shown by the relatively low selectivity sensing elements in artificial noses [29].

There is one additional concern. Despite the differences in ionization mechanism, if an interfering compound has both a higher proton affinity and a lower ionization potential than the analyte, it will lead to a measurable signal with both ionization methods, and if the concentration is high enough, possibly even masking of the analyte signal. From Fig. 4, we see that high molecular weight secondary and tertiary amines such as diazabicyclooctane along with nitrogen-containing heterocyclic aromatic compounds such as acridine and dibenzacridine have these characteristics; as mentioned earlier, the latter of these are known to be present in moderate levels in many petroleum-based products and hence represent the key source of interference when testing in environments rich in these materials. One possible way to overcome this limitation would be to add additional IMS detector channels employing dopant chemistries with even higher values of proton affinity and/or lower values of ionization potential [11]. Although this approach may not be practical due to the size and power requirements of field instruments, recent advances in micro-machined ion mobility drift tubes [30] suggests that massively parallel IMS-based "artificial noses" may someday be possible.

5. Conclusions

The response characteristics of ion mobility spectrometry using two different methods of atmospheric-pressure ionization have been evaluated and compared. The two types of reactive ions were the $[M + 1]^+$ ion formed from ammonia and used for proton exchange (Am-CI) and the laser-generated $M^{\bullet +}$ radical cation of naphthalene used to initiate electron exchange (MPI-CE). These two methods of ionization yielded different response characteristics that were dominated by the thermodynamics of their respective dopant–analyte ion chemistry, and could potentially be combined in a single instrument to enhance noise rejection. A simple model was presented that provides estimates for signal strength (at fixed concentration) as a function of the differences in ionization probabilities (proton affinity or ionization potential) between the dopant and the analyte.

Acknowledgements

This work was sponsored in part by SPAWAR/ONDCP and in part by the Lincoln Laboratory Advanced Concepts Committee, the latter of which is supported principally by the Department of the Air Force under contract F19628-00-C-0002.

References

[1] G.A. Eiceman, Z. Karpas, Ion Mobility Spectrometry, CRC Press, Boca Raton, FL, 1994 (Chapter 1).
[2] W. McGann, Proc. SPIE 2937 (1997) 78.
[3] W. McGann, A. Jenkins, K. Ribiero, J. Napoli, Proc. SPIE 2092 (1993) 64.
[4] R.K. Ritchie, P.C.P. Thomson, R.F. DeBono, L. Danylewich-May, L. Kim, Proc. SPIE 2092 (1993) 87.
[5] G.A. Eiceman, Ion Mobility Spectrometry, CRC Press, Boca Raton, FL, 1994 (Chapter 6).
[6] J.E. E. Roehl, Appl. Spectrsc. Rev. 26 (1991) 1.
[7] C.-W. Su, S. Rigdon, K. Babcock, T. Noble, C. Ranslem, Proc. 1999 ONDCP Int. Technol. Symp., 8–10 March 1999, Washington, DC, p. 1.
[8] G.A. Eiceman, V.J. Vandiver, Anal. Chem. 58 (1986) 2331.
[9] G.A. Eiceman, Ion Mobility Spectrometry, CRC Press, Boca Raton, FL, 1994 (Chapter 2).
[10] R.R. Kunz, J.J. Zayhowski, P. Becotte-Haigh, W.J. McGann, Proc. ONDCP Int. Technol. Symp., Washington, DC, 1999, p. 9.
[11] Q. Meng, Z. Karpas, G.A. Eiceman, Int. J. Environ. Anal. Chem. 61 (1995) 81.
[12] C.S. Leasure, M.E. Fleischer, G.K. Andersen, G.A. Eiceman, Anal. Chem. 58 (1986) 2142.
[13] M.A. Baim, R.L. Eatherton, H.H. Hill Jr., Anal. Chem. 55 (1983) 1761.
[14] D.M. Lubman, M.N. Kronick, Anal. Chem. 54 (1982) 1546.
[15] D.M. Lubman, M.N. Kronick, Anal. Chem. 55 (1983) 1486.
[16] G.A. Eiceman, V.J. Vandiver, C.S. Leasure, G.K. Andersen, J.J. Tiee, W.C. Danen, Anal. Chem. 58 (1986) 1690.

[17] S.C. Subba Rao, C. Fenselau, Anal. Chem. 50 (1978) 511.
[18] S.G. Lias, J.F. Leibman, R.D. Levin, J. Phys. Chem. Ref. Data 13 (1984) 695.
[19] R.D. Levin, S.G. Lias, Ionization Potentials and Appearance Potential Measurements, 1971–1981, National Bureau of Standards, October 1982.
[20] J.J. Zayhowski, C. Dill III, Opt. Lett. 19 (1994) 1427.
[21] U. Boesl, H.J. Neusser, E.W. Schlag, Chem. Phys. 55 (1981) 193.
[22] J.J. Zayhowski, Laser Focus World 35 (1999) 129.
[23] J.P. Reilly, K.L. Kompa, J. Chem. Phys. 73 (1980) 5468.
[24] U. Boesl, H.J. Neusser, E.W. Schlag, Chem. Phys. Lett. 31 (1975) 1.
[25] D.M. Lubman, R. Naaman, R.N. Zare, J. Chem. Phys. 72 (1980) 3034.
[26] R.M. Silverstein, G.C. Bassler, T.C. Morrill, Spectrometric Identification of Organic Compounds, Wiley, New York, 1981, p. 327.
[27] R.B. Bernstein, J. Phys. Chem. 86 (1982) 1176.
[28] Z. Karpas, Z. Berant, O. Shahal, Int. J. Mass Spectrom. Ion Process. 96 (1990) 291.
[29] A.J. Matzger, C.E. Lawrence, R.H. Grubbs, N.S. Lewis, J. Comp. Chem. 2 (2000) 301.
[30] R.A. Miller, E.G. Nazarov, G.A. Eiceman, A.T. King, Sens. Actuators A 91 (2001) 301.